Journal of Medicinal Chemistry

Article

pubs.acs.org/jmc

Dynamic Combinatorial Mass Spectrometry Leads to Inhibitors of a 2-Oxoglutarate-Dependent Nucleic Acid Demethylase

Esther C. Y. Woon,[†,∥] Marina Demetriades,[†,⊥] Eleanor A. L. Bagg,[†,⊥] WeiShen Aik,[†,⊥] Svetlana M. Krylova,[‡,⊥] Jerome H. Y. Ma,[†] MunChiang Chan,[†] Louise J. Walport,[†] David W. Wegman,[‡] Kevin N. Dack,[§] Michael A. McDonough,[†] Sergey N. Krylov,[‡] and Christopher J. Schofield*[,†]

[†]Chemistry Research Laboratory, Department of Chemistry, University of Oxford, 12 Mansfield Road, Oxford, OX1 3TA, United Kingdom

[‡]Department of Chemistry and Centre for Research on Biomolecular Interactions, York University, Toronto, Ontario, M3J 1P3, Canada

[§]Department of World-Wide Medicinal Chemistry, Pfizer PharmaTherapeutics Division, Sandwich, CT 13 9NJ, United Kingdom

Supporting Information

ABSTRACT: 2-Oxoglutarate-dependent nucleic acid demethylases are of biological interest because of their roles in nucleic acid repair and modification. Although some of these enzymes are linked to physiology, their regulatory roles are unclear. Hence, there is a desire to develop selective inhibitors for them; we report studies on AlkB, which reveal it as being amenable to selective inhibition by small molecules. Dynamic combinatorial chemistry linked to mass spectrometric analyses (DCMS) led to the identification of lead compounds, one of which was analyzed by crystallography. Subsequent structure-guided studies led to the identification of inhibitors of improved potency, some of which were shown to be selective over two other 2OG oxygenases. The work further validates the use of the DCMS method and will help to enable the development of inhibitors of nucleic acid modifying 2OG oxygenases both for use as functional probes and, in the longer term, for potential therapeutic use.

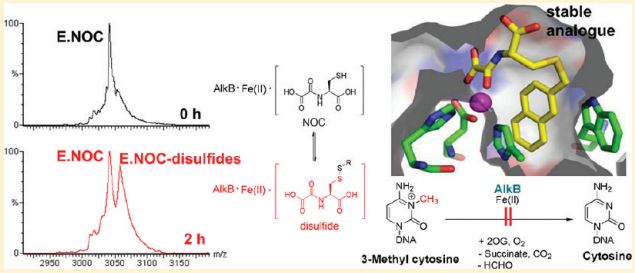

INTRODUCTION

Alkylating agents, of both endogenous and exogenous origins, are constantly modifying nucleic acids in cells, most commonly by methylation. Some of these alkylating modifications are damaging lesions and can lead to mutations, while others are enzyme catalyzed, for example, the formation of 5-methylcytosine, and are regulatory.[1,2] In recent years, it has become apparent that a subfamily of Fe(II)- and 2-oxoglutarate (2OG)-dependent oxygenases catalyzes the hydroxylation of the methyl groups of methylated nucleic acids, which in the case of *N*-methyl-modified DNA/RNA leads to demethylation and thus repair. The first of these enzymes to be identified was *Escherichia coli* AlkB,[3] which is expressed in response to S_N2 type alkylating agents.[4] AlkB acts on a variety of lesions on DNA and RNA but preferentially removes *N*-methyl groups from 1-methyladenine or 3-methylcytosine in single-stranded DNA.[5] This is achieved by oxidizing the *N*-methyl group to a hydroxymethyl group, which is coupled to the conversion of 2OG and O_2 to succinate and CO_2, respectively. The hydroxymethyl intermediate then fragments to give formaldehyde and the unmodified base adenine and cytosine, respectively (Figure 1).[6] Structurally similar lesions are also repaired by AlkB, albeit less efficiently,[7,8] including 1-methylguanine, 3-methylthymine, ethyl, propyl, hydroxyethyl, and hydroxypropyl DNA adducts and exocyclic etheno and ethano adducts, such as 1,N^6-ethenoadenine, 3,N^4-ethenocytosine, and 1,N^2-ethenoguanine.

Eight human homologues (ALKBH1−8) of AlkB have been identified,[9] with ALKBH2 and ALKBH3 being shown to catalyze nucleic acid *N*-demethylation;[9] there is also evidence that ALKBH2 functions as a repair enzyme in vivo.[10] ALKBH8 catalyzes the modification of tRNA.[11] The fat mass and obesity gene (*FTO*) is linked to obesity by genome wide association studies[12] and has been shown to be a nucleic acid demethylase acting on 3-methylthymine in single-stranded DNA[13] and RNA.[14] Recently, the TET (Ten-Eleven-Translocation) enzymes have been reported to catalyze hydroxylation of 5-methylcytosine to give 5-hydroxymethylcytosine[15] and 5-carboxycytosine bases (Figure 1).[16] In some CpG regions, the level of TET-catalyzed modification is a substantial fraction of the total 5-methylcytosine-modified DNA, leading to speculation that TET-catalyzed modifications may be regulatory either by recruitment/loss of binding to regulatory proteins and/or by a direct biophysical effect.[17] Despite some physiological connections (notably for FTO) with the exception of AlkB itself and possibly ALKBH2, the exact molecular roles of the nucleic acid-modifying 2OG-oxygenases

Received: October 20, 2011
Published: January 23, 2012

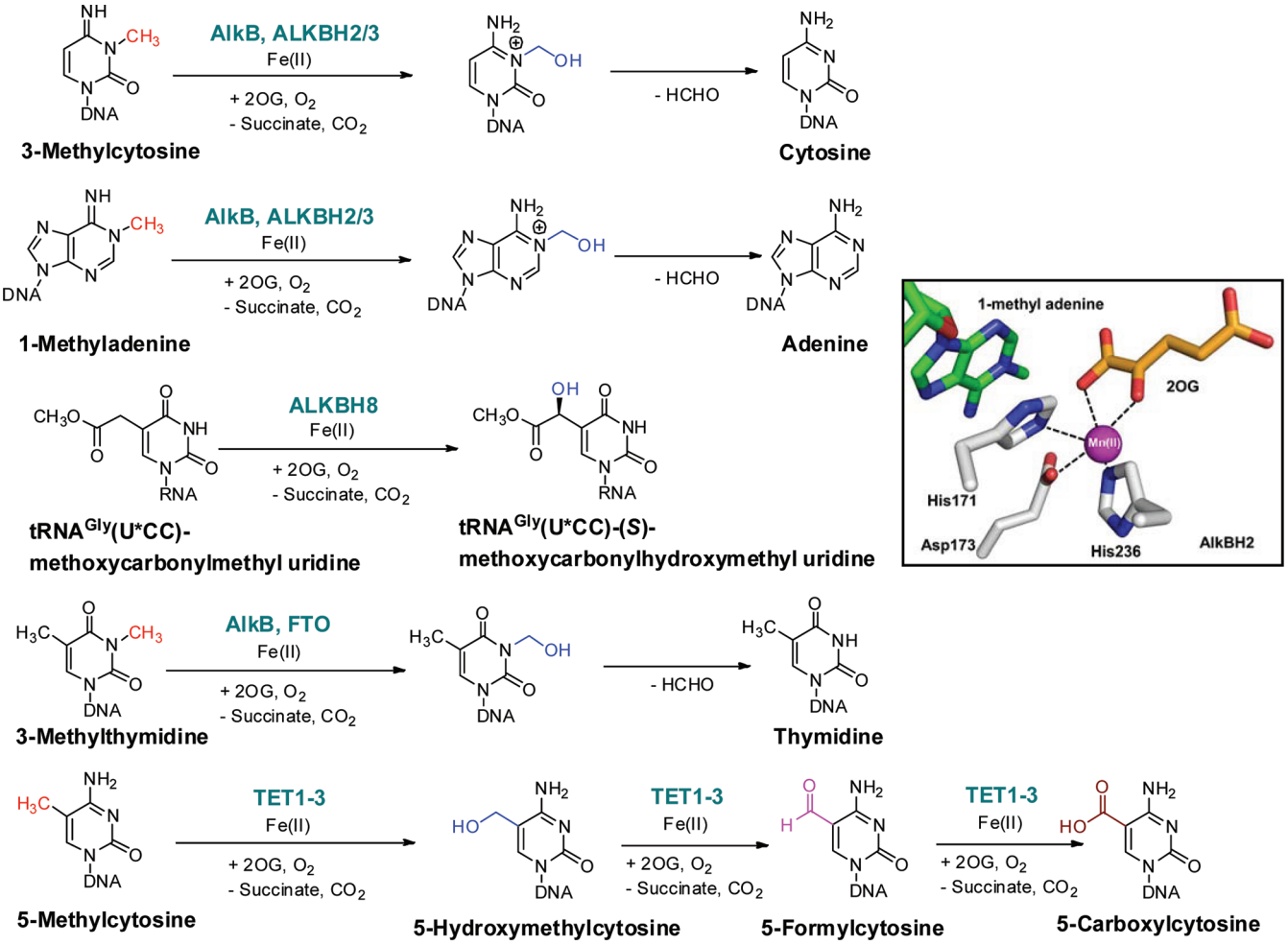

Figure 1. Reactions catalyzed by 2OG-dependent oxygenases that modify nucleic acids. In the repair of 3-methylcytosine and 1-methyladenine lesions by AlkB and ABH2/3, the methyl group is first oxidized to a hydroxymethyl group, which fragments to give formaldehyde and the demethylated base. Methylated RNA as well as DNA may be a substrate in some cases.[7,10] The insert shows a view from a crystal structure of ALKBH2, showing the active site with Mn(II) substituting for Fe(II) (PDB ID: 3BUC).

are unclear. In many cases, they contain additional domains to the catalytic domain (e.g., the C-terminal helical domain of FTO and CXXC domain in the TET enzymes). Thus, the dissection of the nucleic acid modulating roles by genetic means might be problematic. We are therefore interested in aiding the development of small molecule probes that target their catalytic domains.

Here, we report the use of a combined approach employing nondenaturing mass spectrometry binding assays, disulfide-based dynamic combinatorial mass spectrometry (DCMS), crystallographic analyses, fluorescence-based thermal shift assays, and enzyme assays, which led to the identification of *N*-oxalyl-L-cysteine derivatives **1** and 3-hydroxypyridine carboxamides **2** as potent inhibitors of AlkB. Some of these compounds also demonstrated selectivity against other Fe(II)- and 2OG-dependent oxygenases. The results should help to enable the development of functional probes for nucleic acid-modifying 2OG oxygenases.

RESULTS AND DISCUSSION

To explore the tractability of the AlkB enzyme for small molecule inhibition, we initially employed a disulfide-based DCMS screen. We have employed this technique to 2OG-dependent histone demethylases[18] and metallo β-lactamases;[19,20] Poulsen has also applied DCMS to bovine carbonic anhydrase II inhibition.[21] In the DCMS technique, a "support-ligand" that binds to the active site and contains a thiol side chain is allowed to react reversibly (either at the active site or in solution) with a set of thiols to form a mixture of disulfides. Nondenaturing electrospray ionization mass spectrometry (ESI-MS) of the protein−disulfide complexes is then used to identify preferentially binding disulfides. For proteins that are amenable to nondenaturing ESI-MS analysis, this method can provide a rapid means of assessing the relative binding strengths of ligands. In interpreting the nondenaturing ESI-MS analyses, it is important to appreciate that different types of noncovalent interaction survive the transition from solution to gas phase differently.[22] However, in the examples given above, reasonable agreement between results from nondenaturing ESI-MS binding data and those from solution-phase data was observed.

N-Oxalylglycine (NOG) is a reasonably "generic" inhibitor of 2OG oxygenases, but there is evidence that *N*-oxalyl derivatives of other amino acids can display selectivity for different subfamilies.[23,24] Hence, we began by using nondenaturing ESI-MS to test for binding of NOG **3** and a set of L- (**4a**−**d**) and D- (**5a**−**d**) enantiomers of *N*-oxalyl derivatives of amino acids (Figures 2 and 3) to AlkB. Throughout this work, full-length *E.*

dx.doi.org/10.1021/jm201417e | J. Med. Chem. 2012, 55, 2173−2184

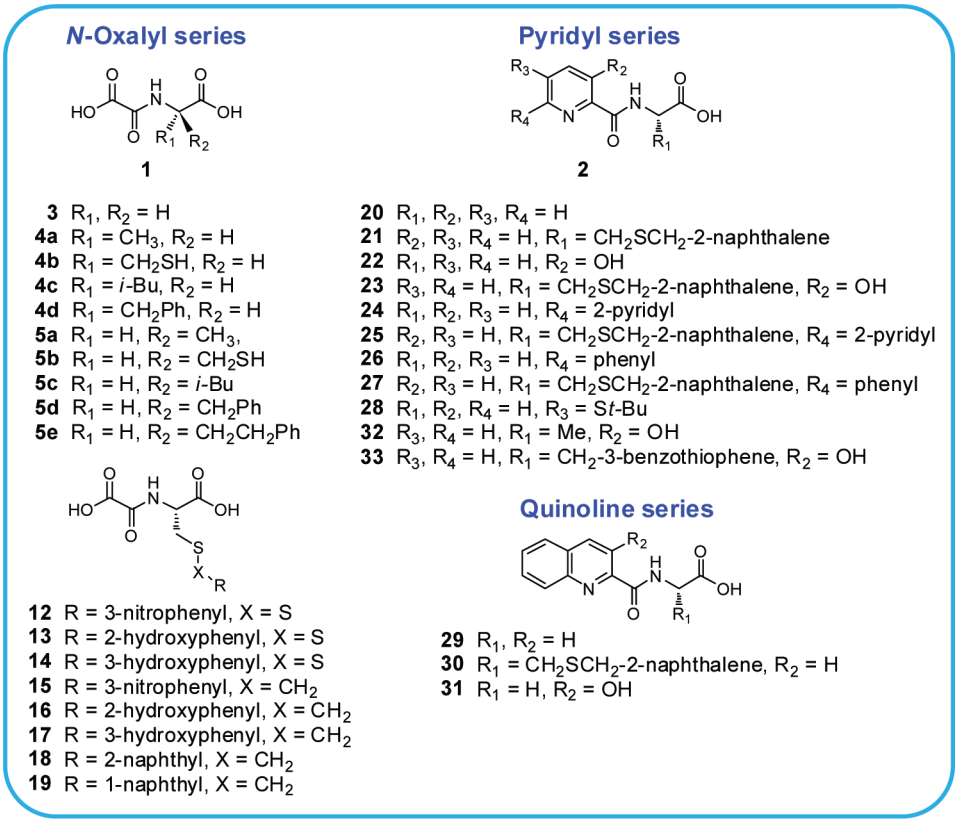

Figure 2. Structures of potential inhibitors investigated in this study.

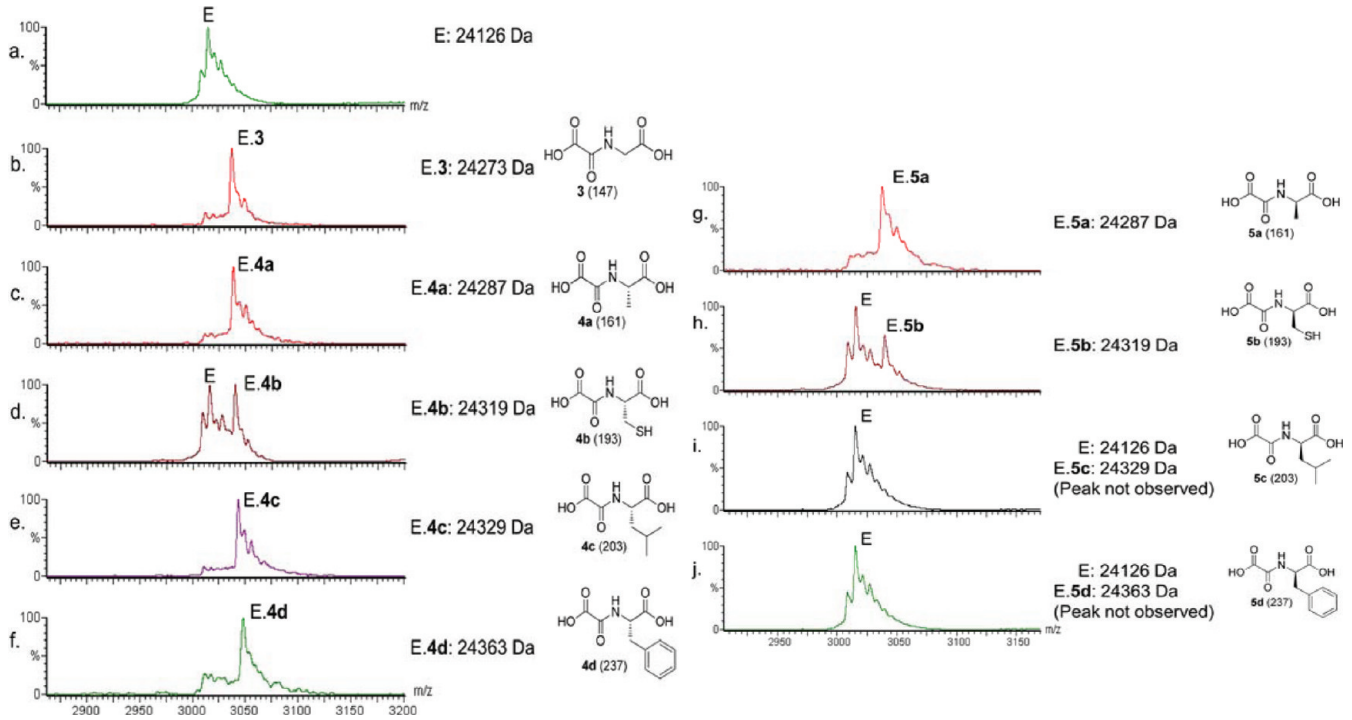

Figure 3. Nondenaturing ESI-MS-based binding assays of *N*-oxalylamino acids to AlkB at 50 V. AlkB·Fe(II) (labeled E) in the presence of (a) no compound, and compounds (b) *N*-oxalyl-L-glycine (NOG) **3**, (c) *N*-oxalyl-L-alanine **4a**, (d) *N*-oxalyl-L-cysteine **4b**, (e) *N*-oxalyl-L-leucine **4c**, (f) *N*-oxalyl-L-phenylalanine **4d**, (g) *N*-oxalyl-D-alanine **5a**, (h) *N*-oxalyl-D-cysteine **5b**, (i) *N*-oxalyl-D-leucine **5c**, and (j) *N*-oxalyl-D-phenylalanine **5d**. Molecular masses (Da) are given in parentheses. A 5-fold excess of Fe(II) was used to give a substantial peak for the AlkB·Fe(II) complex; m/z = mass/charge (Da), z = 8.

coli AlkB was used for nondenaturing ESI-MS binding studies while ΔN11 AlkB,[25] a crystallizable and active form of the AlkB lacking the first 11 *N*-terminal amino acids, was used for enzyme assays, thermal shift assays, and crystallography. The

dx.doi.org/10.1021/jm201417e | J. Med. Chem. 2012, 55, 2173–2184

ESI-MS results were in good agreement with differential scanning fluorimetry (DSF or "thermal shift") assays that indirectly measure the effect of ligands on protein stability;[26] that is, those compounds observed to bind strongly by ESI-MS (e.g., **3**, **4a**,**c**,**d**, and **5a**) gave higher thermal shifts than those that were not observed to bind strongly or not at all (e.g., **4b**, **5b**−**d**) (Figure 3 and Table 1).

Table 1. Activity and Thermal Shifts of the Oxalyl Series against Alkb

Compound	R1	R2	T_m shift/ °C	IC_{50}/ μM
3	H	H	2.9	32
4a	CH_3	H	3.8	35
4b	CH_2SH	H	-1.2	>1mM
4d	CH_2Ph	H	4.3	75
5a	H	CH_3	2.9	149
5b	H	CH_2SH	-1.2	>1mM
5d	H	CH_2Ph	1.0	260
15	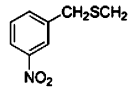	H	4.0	5.2
16	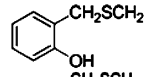	H	1.3	50.4
17	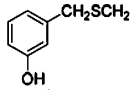	H	1.8	48
18	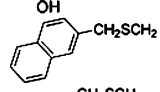	H	7.8	0.5
19	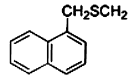	H	3.8	5.4

We then used a capillary electrophoresis-based assay[27,28] to measure IC_{50} values for the *N*-oxalyl amino acid derivatives (Table 1). Again, a good correlation of the rankings of AlkB inhibition potencies with the rankings for ESI-MS binding strength [Kendall's t_b = 0.81 (p < 0.0001), Spearman's ρ = 0.89 (p < 0.0001)] and the rankings for thermal shift [Kendall's t_b = 0.64 (p < 0.0001), Spearman's ρ = 0.67 (p < 0.0001)] were observed. Indeed, throughout the study, with a few exceptions, a good correlation between the results of the three assay methods (ESI-MS, thermal shift, and IC_{50} values) was observed as shown by statistical analyses (Figure S1 in the Supporting Information). These initial results were interesting because they imply that when the C_α substituent is sufficiently large, only the L-enantiomers bind efficiently to AlkB. The apparently preferential binding of the L-enantiomer of *N*-oxalyl amino acids to AlkB is notable because the 2OG-dependent asparaginyl-hydroxylase FIH (factor inhibiting hypoxia inducible factor)[24] and, at least some of the JmjC N^ε-methyl lysine histone demethylases, selectively bind the D-enantiomers of *N*-oxalyl amino acid derivatives.[18,29] Accordingly, we concluded that modifications at the C_α position of L-*N*-oxalyl amino acid may enhance inhibition and enable selectivity.

To explore the extent of the subpocket that is accessible to the *N*-oxalyl amino acid series, a DCMS screen was then performed, using *N*-oxalyl-L-cysteine **4b** as the "support ligand" (Figure 4). A library of 37 thiols (each at 15 μM, Figure 4c) was mixed with **4b** (15 μM), AlkB (15 μM), and Fe(II) (75 μM) in ammonium acetate (15 mM, pH 7.5), under aerobic conditions. The mixture was then analyzed for binding to AlkB by nondenaturing ESI-MS over time. At t_0, the major peak apparent corresponds to the AlkB·Fe(II)·**4b** complex (Figure 5a). After a 1 h incubation, a group of peaks corresponding to the binding of AlkB·Fe(II) to disulfides was apparent (Figure 5b). After 4 h, the AlkB·Fe(II)·**4b** complex almost disappeared, and two main groups of peaks at 24443 and 24472 Da were apparent, presumably reflecting a shift towards formation of the more stable complexes (Figure 5e). These masses correspond to the addition of thiols with molecular masses of ∼124 and ∼153 Da, respectively, and could represent 16 of the 37 thiols in the library (Figure 4c, highlighted in red). Further ESI-MS binding experiments with the 16 individual thiols determined the identity of the bound disulfides to be **4b**·3-nitrothiophenol (**12**), **4b**·2-hydroxythiophenol (**13**), and **4b**·3-hydroxythiophenol (**14**) (Figure 2 and Figure S2 in the Supporting Information). The DCMS screen was then repeated using *N*-oxalyl-D-cysteine **5b** as the "support" ligand (Figure 5g). No AlkB·disulfide complexes were observed, demonstrating stereoselectivity in disulfide recognition by AlkB, that is, a preference for the *N*-oxalyl-L-amino acids. Moreover, AlkB has four cysteine residues within or close to its active site,[25] which can potentially form disulfides with thiols. Therefore, an experiment where the "support ligand" **4b** was excluded from the reaction mixture was performed. No binding of thiols was observed (Figure 5h), demonstrating that the mass shifts observed are likely due to binding of support ligand-based disulfides to AlkB, rather than simultaneous separate binding of **4b** and thiols on the enzyme.

Stable carbon analogues, **15**−**17**, of identified disulfide "hits" **12**−**14**, respectively, wherein the disulfide bond is replaced with a C−S bond, were then synthesized (Figure 2 and Scheme 1). ESI-MS binding experiments implied strong binding of all three carbon analogues to AlkB, with **15** ranking first in binding affinities among the three in pairwise competitive binding experiments (Figure S3 in the Supporting Information). These results are in agreement with those obtained from inhibition and thermal shift assays, which give the following order of inhibitions and melting temperature (T_m) shifts: **15** (IC_{50} = 5.2 μM, T_m shift = 4.0 °C) > **17** (IC_{50} = 48 μM, T_m shift = 1.8 °C) > **16** (IC_{50} = 50.4 μM, T_m shift = 1.3 °C) (Table 1). Binding of the carbon analogues to AlkB, as determined by nondenaturing ESI-MS, was unaffected by an increase in the Fe(II) concentration in the assays; hence, the observed inhibition is unlikely to be a result of Fe(II) chelation in solution.

To investigate the mode of binding of **15** to AlkB, we then carried out crystallographic analyses (PDB ID: 3T4H; Figures 6a and S4a in the Supporting Information). As in previous AlkB structures, when complexed with **15**, the active site iron is coordinated by the side chains of His131 (2.2 Å), Asp133 (2.2 Å), His187 (2.2 Å), and a putative water molecule located *trans* (2.1 Å) to His131. The iron is coordinated by the oxalyl group of **15** in a bidentate manner, with the carboxamide oxygen of **15** (2.2 Å) *trans* to Asp133 and one of the carboxylate oxygens of **15** (2.6 Å) *trans* to His187. The carboxylate oxygen, which is not chelating the iron, is positioned to form hydrogen bonds with the side chain nitrogen NH_2 of Arg210 (3.3 Å) and the side chain oxygen of Asn120 (3.2 Å). The other carboxylic acid of **15** is positioned to form a salt bridge to Arg204 (2.9 and 3.0 Å) and to form hydrogen bonds with the hydroxyl group of

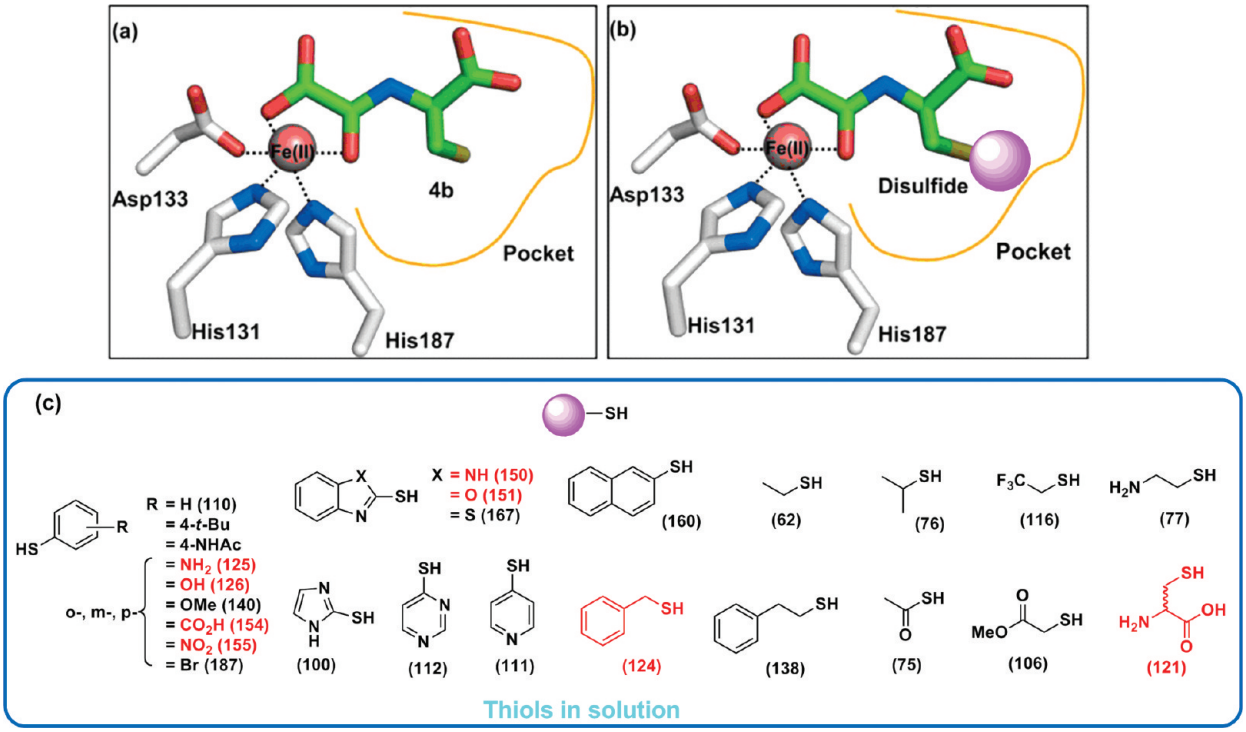

Figure 4. DCMS approach applied to AlkB. (a) The *N*-oxalyl group of support ligand *N*-oxalyl-L-cysteine **4b** anchors it into the active site of AlkB via interaction with the Fe(II) ion (salmon), leaving the thiol side chain free for disulfide formation with thiols in solution (disulfides formed in solution may also bind). (b) Selective formation of an AlkB−disulfide complex involving the thiol member (pink sphere) that fits best into the active site. (c) Structures and molecular masses (in parentheses) of the thiols used. The thiols that have masses corresponding to the observed mass shifts relative to the AlkB·**4b** complex, in the DC-MS analyses are in red.

Tyr122 (2.7 Å) and to the side chain oxygen of Asn206 (2.7 Å). An overlay of this structure with that of AlkB in complex with 2OG (PDB ID: 3I3Q)[30] reveals little difference in the overall conformation of the active site residues [Figure S5 in the Supporting Information, rmsd (all atoms) = 1.3 Å, rmsd (C_α) = 0.7 Å] except for the side chain position of Trp178, which is observed to rotate slightly with respect to its position in the 2OG complex structure, presumably to enable an apparent π-stacking interaction between the phenyl ring of **15** and the side chains of His187 and Trp178, the former being one of the residues involved in Fe(II) coordination (Figure S5 in the Supporting Information). The navigation of the phenyl ring of **15** into a hydrophobic subpocket (defined by Ile143, Phe154, Trp178, Ser182, and His187) is made possible through the relatively flexible cysteinyl linker. The complex is further stabilized by apparent hydrogen-bonding interactions between the 3-nitro group of **15** and the backbone carbonyl oxygen of Ser182 (3.3 Å). Modeling studies suggest that similar interactions are not possible when the 3-nitro group is replaced with a 2-hydroxyl group or a 3-hydroxyl group, possibly explaining the lower inhibitory potencies of **16** (IC_{50} = 50.4 μM) and **17** (IC_{50} = 48 μM), respectively, as compared to **15** (IC_{50} = 5.2 μM).

To take advantage of the apparent hydrophobic subpocket identified in the crystallographic analyses, analogues with naphthalene side chains, **18** and **19**, were proposed as improved inhibitors (Table 1). These were synthesized according to Scheme 1 (for synthetic details, see the Experimental Section and Supporting Information). Consistent with this prediction, the presence of a 2-naphthalene and 1-naphthalene side chain in **18** (IC_{50} = 0.5 μM) and **19** (IC_{50} = 5.4 μM), respectively, increases potency as compared to their parent compound **3** (NOG, IC_{50} = 32 μM) (Table 1). A crystal structure of AlkB in complex with the methylated trinucleotide substrate T-meA-T (PDB ID: 2FD8)[25] reveals close proximity of the nucleotide-binding site (a deep, predominantly hydrophobic pocket) to the 2OG-binding site, wherein the 1-methyladenine base is sandwiched between Trp69 and His131 (Figure S6 in the Supporting Information). Superimposition of the AlkB:T-meA-T complex with that of AlkB:**15** indicates that further elaboration of the oxalyl group of **15**, through replacement with an appropriately substituted pyridyl or quinoline ring, to partially occupy the nucleotide-binding site, would be likely to interfere with the binding of both the nucleotide and the 2OG simultaneously, thereby potentially improving inhibitory potency. Hence, two further series of compounds, the pyridyl (**20**−**28**) and quinoline (**29**−**31**) series, were investigated (Figure 2, Table 2, and Schemes 2 and 3).

The stabilizing effect of the 2-naphthalene side chain is apparent in the pyridyl and quinoline series. With the exception of **23** (IC_{50} = 7.9 μM) and **22** (IC_{50} = 3.4 μM), compounds with the 2-naphthalene side chain were found to be more potent than those without; hence, **21** (IC_{50} = 17.8 μM), **25** (IC_{50} = 16.7 μM), **27** (IC_{50} = 14.7 μM), and **30** (IC_{50} = 22.3 μM) were more potent than **20** (IC_{50} >1 mM), **24** (IC_{50} = 51.3 μM), **26** (IC_{50} = 54.1 μM), and **29** (IC_{50} = 165 μM), respectively (Table 2). The ranking of AlkB inhibition by turnover assays correlates well with the rankings both for thermal shift [Kendall's t_b = 0.67 (p < 0.0001), Spearman's ρ = 0.84 (p < 0.0001)] and for ESI-MS binding strength [Kendall's t_b = 0.80 (p < 0.0001), Spearman's ρ = 0.90 (p < 0.0001), Figure S1 in the Supporting Information], hence validating the use of these techniques as efficient and rapid methods in screening for 2OG oxygenase inhibitors.

dx.doi.org/10.1021/jm201417e | J. Med. Chem. 2012, 55, 2173−2184

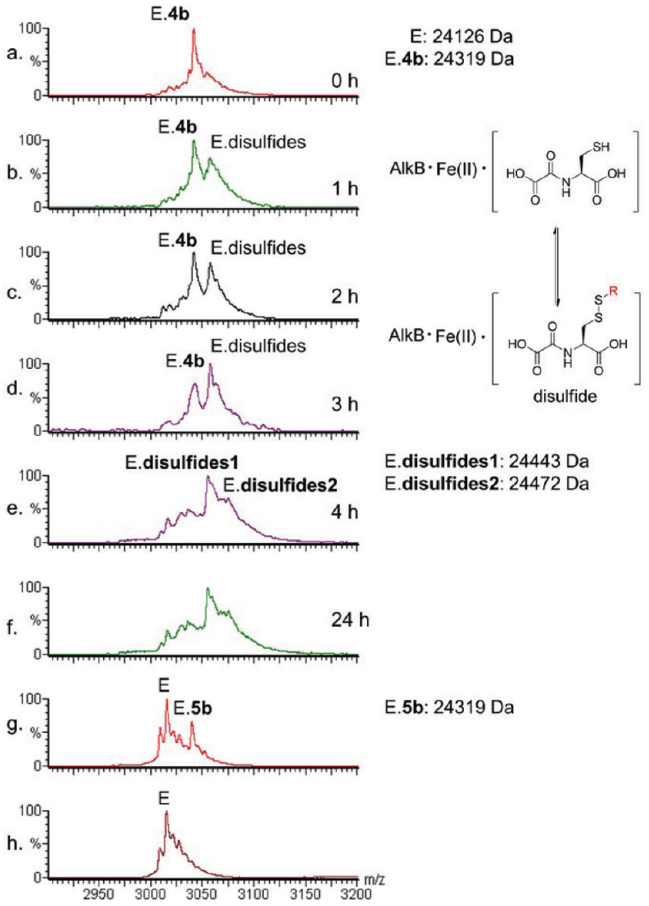

Figure 5. Dynamic combinatorial mass spectrometric (DCMS) analyses on AlkB. Nondenaturing ESI-MS spectra at 30 V showing AlkB·Fe(II) (labeled E) in the presence of (a) *N*-oxalyl-L-cysteine **4b** and the thiol library at 0, (b) 1, (c) 2, (d) 3, (e) 4, and (f) 24 h; (g) AlkB·Fe(II) in the presence of *N*-oxalyl-D-cysteine **5b** and the thiol library at 24 h; and (h) AlkB·Fe(II) in the presence of the thiol library at 24 h without *N*-oxalyl-L-cysteine **4b**. m/z = mass/charge (Da), z = 8.

Interestingly, a crystal structure of the most potent compound **18** (IC_{50} = 0.5 μM, T_m shift = 7.8 °C) in complex with AlkB was then obtained (PDB ID: 3T4V; Figures 6b and S4b in the Supporting Information). The oxalyl group of **18** is observed to coordinate with iron in a manner analogous to that of 2OG and **15** (Figures 6a and S3a in the Supporting Information) with most apparent salt bridges and hydrogen bonds in the AlkB:**15** complex being conserved. The cysteinyl linker of **18**, however, adopts a different conformation from that of **15**, likely to align the bulkier 2-naphthalene side chain of **18** with the side chains of His187 and Trp178 for efficient π-stacking interactions. Analysis of the AlkB:**18** complex structure suggests that the 1-naphthalene side chain of **19** is less able to fit into the hydrophobic subpocket due to steric constraints, accounting for its lower inhibitory activity (IC_{50} = 5.4 μM) as compared to **18**.

A crystal structure of AlkB in complex with **22** (PDB ID: 3T3Y; Figures 6c and S4c in the Supporting Information) reveals a different mode of binding from those of **15** and **18**, wherein the pyridine ring, instead of occupying the same metal coordinating position as the oxalyl groups in **15** and **18**, "flips" over with the pyridyl nitrogen (2.2 Å) *trans* to His131 to partially occupy the hydrophobic subpocket. The side chain of Trp178 is rotated (approximately 90° about the C_α–C_β bond and approximately 180° about the C_β–C_γ bond) to form π-stacking interactions with the pyridine ring. The 3-hydroxyl group of **22** is positioned to participate in a hydrogen bond to the side chain hydroxyl group of Ser145 (2.1 Å), possibly accounting for the greater potencies of **22** (IC_{50} = 3.4 μM), **23** (IC_{50} = 7.9 μM), and **31** (IC_{50} = 42.5 μM) as compared to analogues without the 3-hydroxyl group **20** (IC_{50} > 1 mM), **21** (IC_{50} = 17.8 μM), and **29** (IC_{50} = 165 μM), respectively.

To investigate the selectivity of the most potent AlkB inhibitors against other Fe(II)- and 2OG-dependent oxygenases, three of the more potent inhibitors (**15**, **18**, and **19**) were tested for inhibition against two physiologically important human 2OG oxygenases PHD2 (hypoxia-inducible factor prolyl hydroxylase 2, which is central to the hypoxic response) and PHF8 (PHD finger protein 8, the mutations to which are linked to midline defects).[31] All three compounds showed IC_{50} > 1 mM for both PHD2[32] and PHF8,[33] which represent significant selectivity (200–2000-fold) towards AlkB.

CONCLUSIONS

Overall, the results demonstrate that AlkB, and by implication other 2OG-dependent nucleic acid-modifying oxygenases, are amenable to potent inhibition by small molecules. The combined results, including crystallographic analyses, should provide a basis for the development of potent and selective AlkB/ALKBH inhibitors, suitable for use as functional probes and, in the longer term, possibly for clinical use. Importantly, the results demonstrate that a high degree of selectivity for AlkB over other subfamilies of 2OG oxygenases should be possible, as shown by a lack of inhibition of our most potent AlkB inhibitors against two other 2OG oxygenases, PHD2 at 1 mM. Notably, in the *N*-oxalyl amino acid compounds, the L-

Scheme 1. Synthesis of the *N*-Oxalyl Inhibitors[a]

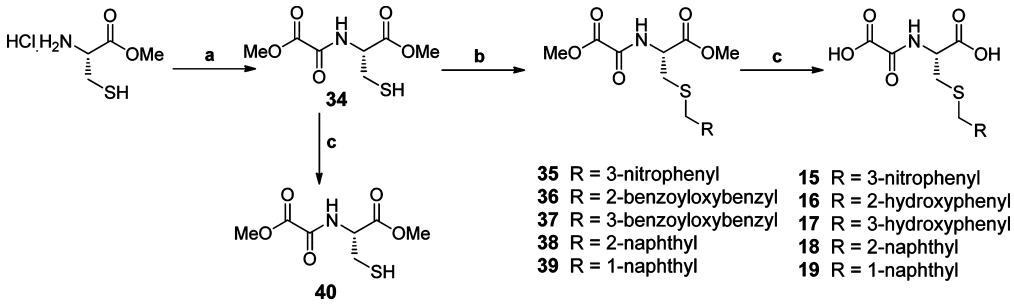

[a]Conditions: (a) Monomethyl oxalyl chloride, Et_3N, CH_2Cl_2. (b) RCH_2Br, Et_3N, CH_2Cl_2. (c) NaOH (1 N), MeOH.

dx.doi.org/10.1021/jm201417e | J. Med. Chem. 2012, 55, 2173–2184

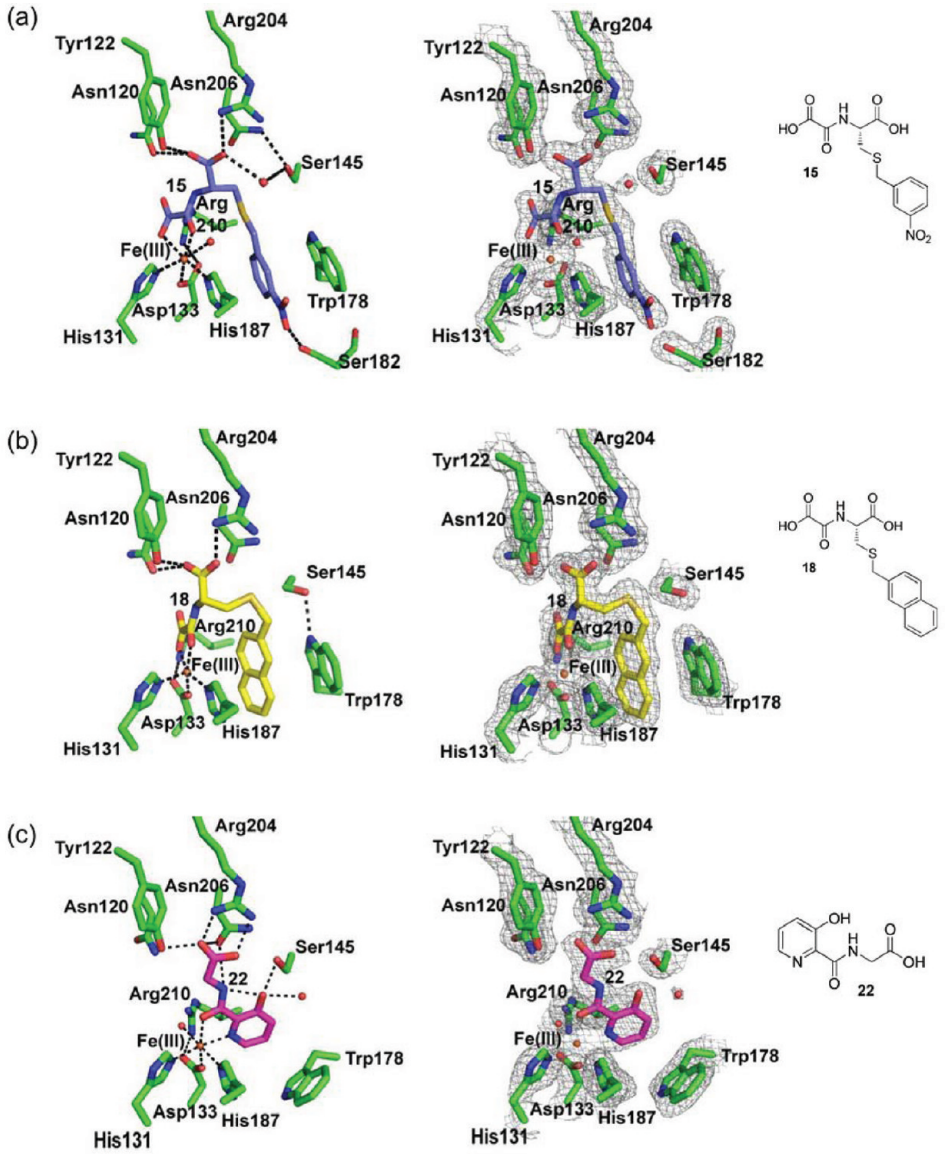

Figure 6. Active site views from structures of AlkB (green sticks) bound to (a) **15** (purple sticks; PDB ID: 3T4H), (b) **18** (yellow sticks; PDB ID: 3T4V), and (c) **22** (magenta sticks; PDB ID: 3T3Y). The experimental $2F_o - F_c$ electron density maps (contoured to 1.5σ), displayed as gray mesh, are shown to the right.

stereochemistry at the C_α center gave preferential inhibition. This contrasts with FIH and the JMJD2 family of histone demethylases, which are selectively inhibited by the D-stereochemistry of related *N*-oxalyl amino acid derivatives.[18,24] Thus, consideration of the stereochemistry of the C_α center (and equivalent in other series) is an important factor in obtaining subfamily selectivity. It should be noted that there are likely considerable variations in the active sites of the ALKBH1−8 and related human enzymes (FTO, TET1−3); thus, further discrimination within the group of nucleic acid-modifying 2OG oxygenases is likely possible. This will be important in developing 2OG oxygenase inhibitors for use as functional probes.

The work also further validates the use of the DCMS method for identifying lead compounds useful for inhibitor development. An advantage of the DCMS binding assay method over most other techniques for the analysis of compound binding is that it directly analyzes the mass of protein−ligand complexes. We observed good correlation between the ESI-MS-based binding results, IC_{50} values, and thermal shift assays. We appreciate that there are limitations to the use of ESI-MS binding assay results, both because not all proteins are suitable for this type of assay and because the strength of binding as observed by the ESI-MS appears to be dependent on the type of interactions involved in binding,[22] likely reflecting the relative contribution of entropic and enthalpic components. The latter consideration means that it can be difficult to compare results between series of compounds that bind differently. Nevertheless, in our work, we saw good correlation between the binding strengths and the assay results and anticipate that, as the empirical data sets accumulate, confidence in the ESI-MS binding assays results will increase.

EXPERIMENTAL SECTION

Chemical Synthesis. Reagents and solvents were from Aldrich or Alfa Aesar. Reactions were monitored by TLC, which was performed on precoated aluminum-backed plates (Merck, silica 60 F254). Melting points were determined using a Leica Galen III hot-stage

dx.doi.org/10.1021/jm201417e | *J. Med. Chem.* 2012, 55, 2173−2184

Table 2. Activity and Thermal Shifts of the Pyridyl Series (20−28, 32, and 33) and Quinoline Series (29−31) against AlkB

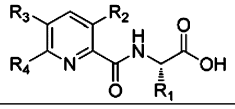

Compound	R1	R2	R3	R4	T_m shift/ °C	IC_{50}/ μM
20	H	H	H	H	0.7	>1mM
21		H	H	H	3.1	17.8
22	H	OH	H	H	8.3	3.4
23		OH	H	H	10.6	7.9
24	H	H	H		0.3	51.3
25		H	H		0.4	16.7
26	H	H	H	Ph	-0.6	54.1
27		H	H	Ph	1.7	14.7
28	H	H	StBu	H	0.6	121
32	Me	OH	H	H	10.0	9.5
33		OH	H	H	3.7	14.1

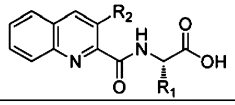

Compound	R1	R2	T_m shift/ °C	IC_{50}/ μM
29	H	H	1.1	165
30		H	2.0	22.3
31	H	OH	5.8	42.5

melting point apparatus and microscope. Infrared spectra were recorded from Nujol mulls between sodium chloride discs, on a Bruker Tensor 27 FT-IR spectrometer. NMR spectra were acquired using a Bruker DPX500 NMR spectrometer. Chemical shifts (δ) are given in ppm, and the multiplicities are given as singlet (s), doublet (d), triplet (t), quartet (q), multiplet (m), and broad (br). Coupling constants J are given in Hz (±0.5 Hz). High resolution mass spectra (HRMS) were recorded using Bruker MicroTOF. The purity of all compounds synthesized was ≥95% as determined by analytical reverse-phase HPLC (Ultimate 3000). The synthesis and characterization of compound **31** and **29** were as reported in refs 34 and 35, respectively. The syntheses of compounds **16**−**17**, **19**−**21**, **23**−**28**, **30**, **32**, and **33** are given in the Supporting Information.

*N-Methyloxalyl-L-cysteine Methyl Ester (**34**).* Monomethyl oxalyl chloride (2.94 mL, 32.0 mmol) was added dropwise to a mixture of L-cysteine methyl ester hydrochloride (5.00 g, 29.1 mmol) and Et_3N (8.9 mL, 64.0 mmol) in anhydrous CH_2Cl_2 (100 mL) at 0 °C. The mixture was then stirred at room temperature for overnight, after which it was evaporated in vacuo. The resulting residue was dissolved in EtOAc, washed (saturated $NaHCO_3$, H_2O, and brine), dried (Na_2SO_4), and evaporated in vacuo. Chromatography (EtOAc/hexane 1:1) gave **34** as a pale yellow oil (6.43 g, quantative yield). R_f = 0.4. IR (neat) υ/cm^{-1}: 3346 (NH), 1743 (CO ester), 1615 (CO amide). ^{1}H NMR (500 MHz, $CDCl_3$): δ 2.90 (1H, dd, J = 6.5, 14.0 Hz, CH_2SH), 2.95 (1H, dd, J = 5.0, 14.0 Hz, CH_2SH), 3.82 (3H, s, CO_2CH_3), 3.93 (3H, s, $COCO_2CH_3$), 4.70−4.75 (1H, m, CH), 7.88 (1H, br s, NH). ^{13}C NMR (500 MHz, $CDCl_3$): δ 26.3 (CH_2SH), 53.1 (CH), 53.8 (CO_2CH_3), 54.1 ($COCO_2CH_3$), 155.9 ($COCO_2CH_3$), 160.2 ($COCO_2CH_3$), 169.3 (CO_2CH_3). HRMS (ESI, positive ion) $C_7H_{11}NNaO_5S$ [M + Na]$^+$ requires 244.0250; found, 244.0253.

*N-Oxalyl-L-cysteine (**40**).* A solution of aqueous NaOH (1 N, 10.00 mL, 10.0 mmol) was added dropwise to a mixture of **34** (0.57 g, 1.7 mmol) in MeOH (20 mL) at 0 °C. The mixture was stirred for 1 h and then allowed to warm to room temperature overnight, after which it was evaporated in vacuo. The resulting residue was resuspended in H_2O, acidified with aqueous HCl (1 N) to pH 2, and extracted with EtOAc. The organic extracts were washed (saturated $NaHCO_3$, H_2O, and brine), dried (Na_2SO_4), and evaporated in vacuo. This gave **40** as a white solid (0.38 g, 73%); mp 159−160 °C. R_f = 0.2 (MeOH/CH_2Cl_2 3:7). IR (neat) ν_{max}/cm^{-1} 3010−3364 (NH and OH), 1645 (amide CO), 1524 (carboxylate CO). ^{1}H NMR (500 MHz, MeOD): δ 3.01 (1H, dd, J = 7.0, 14.0 Hz, CH_2SH), 3.09 (1H, dd, J = 5.0, 14.0 Hz, CH_2SH), 4.67 (1H, dd, J = 4.5, 6.5 Hz, CH). ^{13}C NMR (500 MHz, MeOD): δ 35.4 (CH_2SH), 55.9 (CH), 165.5 ($COCO_2H$), 166.6 ($COCO_2H$), 177.4 (CO_2H). HRMS (ESI, negative ion) $C_5H_6NO_5S$ [M − H]$^-$ requires 191.9972; found, 191.9968.

Synthesis of *N*-Oxalyl Inhibitor 15 and 18. *N-Methyloxalyl-S-(3-nitrobenzyl)-L-cysteine Methyl Ester (**35**).* Triethylamine (2.50 mL, 17.9 mmol) was added dropwise to a solution of **34** (3.04 g, 13.8 mmol) and 3-nitrobenzyl brominde (3.3 g, 15.1 mmol) in anhydrous CH_2Cl_2 (50 mL) at 0 °C. The mixture was stirred for 2 h and then allowed to warm to room temperature overnight, after which it was evaporated in vacuo. The resulting residue was dissolved in EtOAc, washed (saturated $NaHCO_3$, H_2O, and brine), dried (Na_2SO_4), and evaporated in vacuo. Chromatography (EtOAc/hexane 2:3) gave **35** as a colorless oil (2.45 g, 50%). R_f = 0.3. IR (neat) υ/cm^{-1}: 3340 (NH), 1735 (CO ester), 1684 (CO amide) 1525, 1352 (NO_2). ^{1}H NMR (500 MHz, $CDCl_3$): δ 2.89 (1H, dd, J = 6.0, 14.0 Hz, cysteinyl CH_2), 2.97 (1H, dd, J = 5.0, 14.5 Hz, cysteinyl CH_2), 3.78 (3H, s, CO_2CH_3), 3.82 (2H, s, benzyl CH_2), 3.94 (3H, s, $COCO_2CH_3$), 4.76−4.84 (1H, m, CH), 7.51 (1H, t, J = 8.0 Hz, H5′), 7.66 (1H, d, J = 8.0 Hz, H4′), 7.73 (1H, d, J = 8.0 Hz, NH), 8.13 (1H, d, J = 8.0 Hz, H6′), 8.19 (1H, s, H2′). ^{13}C NMR (500 MHz, $CDCl_3$): δ 33.2 (cysteinyl CH_2), 35.8 (benzyl CH_2), 52.0 (CH), 53.1 (CO_2CH_3), 53.9 ($COCO_2CH_3$), 122.4 (C6′), 123.8 (C2′), 129.6 (C5′), 135.0 (C4′), 139.6 (C1′), 148.4 (C3′), 155.9 ($COCO_2CH_3$), 160.2 ($COCO_2CH_3$), 169.9 (CO_2CH_3). HRMS (ESI, positive ion) $C_{14}H_{16}N_2NaO_7S$ [M + Na]$^+$ requires 379.0570; found, 379.0574.

*N-Oxalyl-S-(3-nitrobenzyl)-L-cysteine (**15**).* A solution of aqueous NaOH (1N, 13.00 mL, 13.0 mmol) was added dropwise to a solution of **35** (0.77 g, 2.2 mmol) in THF (20 mL) at 0 °C. The mixture was stirred for 1 h and then allowed to warm to room temperature overnight, after which it was evaporated in vacuo. The resulting residue was resuspended in H_2O, acidified with aqueous HCl (1 N) to pH 2, and extracted with EtOAc. The organic layer was washed (saturated $NaHCO_3$, H_2O, and brine), dried (Na_2SO_4), and evaporated in vacuo. Chromatography (MeOH/CH_2Cl_2 3:7) gave **15** as an off-white solid (0.43 g, 61%); mp 114−115 °C. R_f = 0.4. IR (neat) ν_{max}/cm^{-1} 3016−3353 (NH and OH), 1738 (amide CO), 1654 (carboxylate CO), 1525, 1352 (NO_2). ^{1}H NMR (500 MHz, MeOD): δ 2.93 (1H, dd, J = 7.0, 14.2 Hz, cysteinyl CH_2), 3.05 (1H, dd, J = 5.0, 14.0 Hz, cysteinyl CH_2), 3.93 (1H, s, benzyl CH_2), 4.62−4.69 (1H, m, CH), 7.58 (1H, t, J = 8.0 Hz, H5′), 7.78 (1H, d, J = 8.0 Hz, H4′), 8.14 (1H, d, J = 8.0 Hz, H6′), 8.26 (1H, s, H2′). ^{13}C NMR (500 MHz, MeOD): δ 33.6 (cysteinyl CH_2), 36.3 (benzyl CH_2), 53.8 (CH), 123.2 (C6′), 124.8 (C2′), 130.9 (C5′), 136.5 (C4′), 142.2 (C1′), 149.8 (C3′), 165.3 ($COCO_2H$), 166.2 ($COCO_2H$), 177.5 (CO_2H). HRMS (ESI, positive ion) $C_{12}H_{12}N_2NaO_7S$ [M + Na]$^+$ requires 351.0257; found, 351.0264.

*N-Methyloxalyl-S-(2-naphthalenemethyl)-L-cysteine Methyl Ester (**38**).* Triethylamine (0.4 mL, 2.94 mmol) was added dropwise to a solution of **34** (0.50 g, 2.26 mmol) and 2-bromomethylnaphthalene (0.55 g, 2.49 mmol) in anhydrous CH_2Cl_2 (40 mL) at room temperature. The mixture was stirred at room temperature for 18 h, washed (H_2O), dried ($MgSO_4$), and evaporated in vacuo. Chromatography (hexane/EtOAc 6:4) gave **38** as a white solid (0.36 g, 43%); mp 87−90 °C. R_f = 0.35. $[\alpha]_D$ = −67.1 (c 2.56 × 10^{-3}). IR (neat) ν/cm^{-1}: 3303 (NH), 1735 (CO ester), 1687 (CO amide). ^{1}H NMR (500 MHz, $CDCl_3$): δ 2.91 (1H, qd, J = 5.0, 16.0 Hz,

Scheme 2. Synthesis of Pyridyl Inhibitors[a]

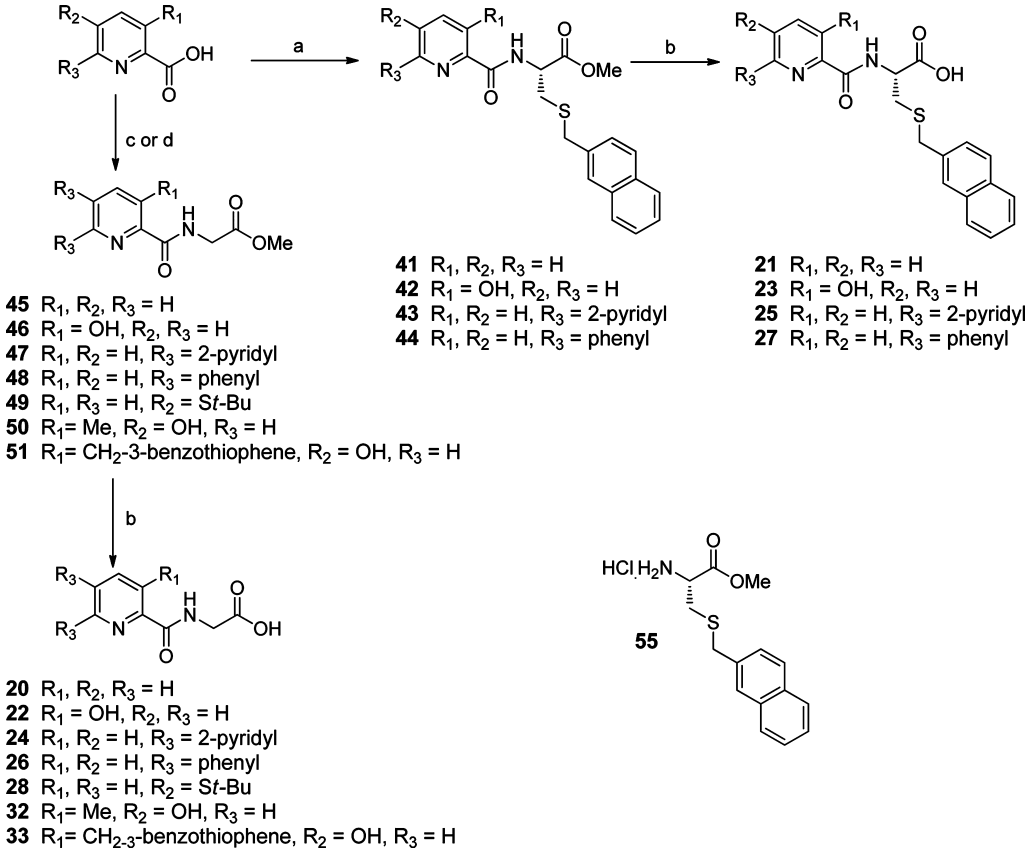

[a]Conditions: (a) Compound **55**, diisopropylethylamine, hydroxybenzotriazole, 1-ethyl-3-(3-dimethylaminopropyl)carbodiimide, CH_2Cl_2. (b) LiOH (1 N), 1,4-dioxane. (c) Glycine methyl ester hydrochloride, diisopropylethylamine, hydroxybenzotriazole, 1-ethyl-3-(3-dimethylaminopropyl)-carbodiimide, CH_2Cl_2. (d) L-Alanine methyl ester hydrochloride or L-tryptophan methyl ester hydrochloride for compounds **50** and **51**, respectively, diisopropylethylamine, hydroxybenzotriazole, 1-ethyl-3-(3-dimethylaminopropyl)carbodiimide, CH_2Cl_2.

Scheme 3. Synthesis of Quinoline Inhibitors[a]

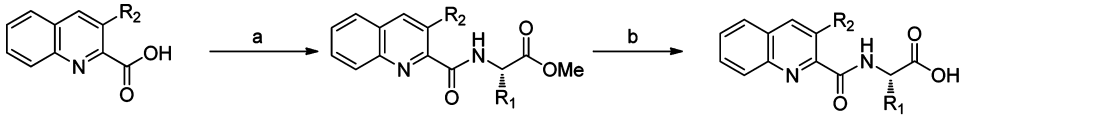

[a]Conditions: (a) Glycine (**40** for compound **53**), diisopropylethylamine, hydroxybenzotriazole, 1-ethyl-3-(3-dimethylaminopropyl)carbodiimide, CH_2Cl_2. (b) LiOH (1 N), 1,4-dioxane.

cysteinyl CH_2), 3.75 (3H, s, CO_2CH_3), 3.88–3.91 (2H, m, cysteinyl CH_2), 3.90 (3H, s, $COCO_2CH_3$), 4.81–4.85 (1H, m, CH), 7.45–7.51 (3H, m, ArC*H*), 7.71 (1H, d, J = 6.5 Hz, ArC*H*), 7.81–7.83 (3H, m, ArC*H*). ^{13}C NMR (500 MHz, $CDCl_3$): δ 32.85 (CH_2), 36.8 (cysteinyl CH_2), 52.0 (CH), 52.9 (CO_2CH_3), 53.8 ($COCO_2CH_3$), 126.0 (Ar CH), 126.3 (Ar CH), 126.8 (Ar CH), 127.6 (Ar CH), 127.7 (Ar CH), 127.7 (Ar CH), 128.6 (Ar CH), 132.6 (Ar C), 133.2 (Ar C), 134.6 (Ar C), 155.9 ($COCO_2CH_3$), 160.2 ($COCO_2CH_3$), 170.0 (CO_2CH_3). HRMS (ESI^+) $C_{18}H_{19}NNaO_5S$ $[M + Na]^+$ requires 384.0876; found, 384.0877.

*N-Oxalyl-S-(2-naphthalenemethyl)-L-cysteine (**18**).* A solution of aqueous NaOH (1 N, 0.9 mL, 0.9 mmol) was added dropwise to a solution of **38** (0.17 g, 0.47 mmol) in MeOH (10 mL) and was stirred at room temperature overnight, after which it was evaporated in vacuo. The resulting residue was resuspended in H_2O, acidified with aqueous HCl (1 N) to pH 2, and extracted with EtOAc. The organic layer was washed (H_2O, brine), dried ($MgSO_4$), and evaporated in vacuo. Washing with Et_2O (3 mL) gave **18** as a white solid (0.07 g, 50%); mp 159–160 °C. $[\alpha]_D = -43.6$ (c 1.01 × 10^{-3}). IR (neat) ν_{max}/cm^{-1} 3309 (N–H), 3235 (COO-H), 1748 (HOC=O), 1726 (C=O), 1639 (NC=O). ^{1}H NMR (500 MHz; MeOD-d_4): δ 2.89–3.05 (2H, m, SCH_2), 3.95 (2H, s, CH_2), 4.68–4.71 (1H, m, CH), 7.46–7.51 (3H, m, ArC*H*), 7.76 (1H, s, Ar C*H*), 7.81–7.84 (3H, m, Ar C*H*). ^{13}C NMR (125 MHz, MeOD-d_4): δ 33.1 (CH_2), 37.2 (CH_2), 53.9 (CH), 126.9 (Ar CH), 127.1 (Ar CH), 127.3 (Ar CH), 128.2 (Ar CH), 128.7 (Ar CH), 129.3 (Ar CH), 129.5 (Ar CH), 134.1 (Ar C), 134.7 (Ar C), 136.6 (Ar C), 172.6 (CO_2H). HRMS (ESI^-) $C_{16}H_{14}NO_5S$ $[M - H]^-$ requires 332.0598; found, 332.0595.

Synthesis of Pyridyl Inhibitor 22. *Methyl 2-(3-Hydroxypicolinamido)acetate (**46**).* To a stirred solution of picolinic acid (0.50 g, 3.59 mmol) in dry CH_2Cl_2 (20 mL) under N_2, hydroxybenzotriazole (0.58 g, 4.31 mmol), 1-ethyl-3-

dx.doi.org/10.1021/jm201417e | J. Med. Chem. 2012, 55, 2173–2184

(3-dimethylaminopropyl) carbodiimide (0.76 mL, 4.31 mmol), and diisopropylethylamine (1.25 mL, 7.18 mmol) were added. The mixture was stirred for 10 min, and glycine methyl ester hydrochloride (0.45 g, 3.59 mmol) was added. The reaction mixture was stirred for 36 h until consumption of starting material. The mixture was washed with water, and the organic layer was dried with $MgSO_4$ and concentrated under reduced pressure. The yellow oil was chromatographed (hexane/EtOAc 7:3 to 5:5). Chromatography gave compound **46** as white needles (0.35 g, 47%); mp 54−55 °C. R_f = 0.36. IR (neat) ν_{max}/cm^{-1} 3355 (O−H, N−H), 1749(OC═O), 1651 (NC═O). ^{1}H NMR (500 MHz; $CDCl_3$): δ 3.79 (3H, s, CH_3), 4.23 (2H, d, J = 6.0, CH_2), 7.28−7.35 (2H, m, Ar C*H*), 8.07 (1H, dd, J = 4.0 1.5, Ar C*H*), 8.46 (1H, s, N*H*), 11.76 (1H, s, O*H*). ^{13}C NMR (125 MHz, $CDCl_3$): δ 40.7 (CH_2), 52.5 (CH_3), 126.05 (Ar *C*H), 128.9 (Ar *C*H), 131.0 (Ar *C*), 139.8 (Ar *C*H), 157.7 (Ar *C*), 169.0 (*C*ONH), 169.6 (CO_2CH_3). HRMS (ESI$^+$) $C_9H_{10}N_2NaO_4$ [M + Na]$^+$ requires 233.0533; found, 233.0525.

*2-(3-Hydroxypicolinamido)acetic Acid (**22**).* To a solution of **46** (0.02 g, 0.095 mmol) in 1,4-dioxane (5 mL), 1 N lithium hydroxide (0.2 mL, 0.2 mmol) was added. The mixture was stirred at room temperature for 24 h until the consumption of starting material and acidified with acetic acid to pH 3 and diluted with CH_2Cl_2. The solution was washed with water, dried ($MgSO_4$), and concentrated in vacuo. Concentration gave compound **22** as a white solid (2.0 mg, 20%); mp 169−170 °C. IR (neat) ν_{max}/cm^{-1} 3354 (O−H, N−H), 2950 (COO-H), 1745 (OC═O), 1678 (NC═O). ^{1}H NMR (500 MHz; DMSO-d_6): δ 4.00 (2H, d, J = 6.0, CH_2), 7.45 (1H, dd, J = 8.5 1.5, Ar C*H*), 7.56 (1H, q, J = 4.0, Ar C*H*), 8.20 (1H, dd, J = 4.5 1.5, Ar C*H*), 9.33 (1H, t, J = 6.0, N*H*), 12.30 (1H, s, O*H*). ^{13}C NMR (125 MHz, DMSO-d_6): δ 40.6 (CH_2), 125.95 (Ar *C*H), 129.35 (Ar *C*H), 130.9 (Ar *C*), 140.0 (Ar *C*H), 157.2 (Ar *C*), 169.0 (*C*ONH), 170.5 (CO_2H). HRMS (ESI$^-$) $C_8H_7N_2O_4$ [M − H]$^-$ requires 195.0411; found, 195.0417.

Synthesis of Quinoline Inhibitor 29. *Methyl 2-(Quinoline-2-carboxamido)acetate (**52**).* Triethylamine (3.31 mL, 23.75 mmol) was added dropwise to a solution of glycine methyl ester hydrochloride (0.13 g, 1.04 mmol) and quinaldoyl chloride (0.20 g, 1.04 mmol) in anhydrous CH_2Cl_2 (20 mL) at room temperature. The mixture was stirred at room temperature for 2 days, washed (H_2O), dried ($MgSO_4$), and evaporated in vacuo. Chromatography (hexane/EtOAc 7:3 to 6:4) gave **52** as a white solid (0.12 g, 50%); mp 98−99 °C. R_f = 0.35. IR (neat) ν_{max}/cm^{-1} 3328 (N−H), 1746 (CH_3OC═O), 1653 (NC═O). ^{1}H NMR (500 MHz; $CDCl_3$): δ 3.83 (3H, s, CH_3), 4.35 (2H, d, J = 6.0, CH_2), 7.62−7.65 (1H, m, Ar C*H*), 7.76−7.80 (1H, m, Ar C*H*), 7.88 (1H, d, J = 4.0, ArC*H*), 8.15 (1H, dd, J = 8.8, 1.0, Ar C*H*), 8.31 (2H, dd, J = 15.0, 8.5, Ar C*H*), 8.71 (1H, t, J = 5.0, N*H*). ^{13}C NMR (125 MHz, $CDCl_3$): δ 41.3 (CH_2), 52.4 (CH_3), 118.8 (Ar *C*H), 127.7 (Ar *C*H), 128.0 (Ar *C*H), 129.4 (Ar *C*H), 129.8 (Ar *C*H), 130.1 (Ar *C*H), 137.5 (Ar *C*), 146.5 (Ar *C*), 149.0 (Ar *C*), 164.8 (*C*ONH), 170.2 (CO_2CH_3). HRMS (ESI$^-$) $C_{13}H_{12}N_2O_3$ [M + Na]$^-$ requires 267.0740; found, 267.0731.

*2-(Quinoline-2-carboxamido)acetic Acid (**29**).*[35] To a solution of **52** (25 mg, 0.10 mmol) in 1,4-dioxane (3 mL), 1 N lithium hydroxide (0.20 mL, 0.20 mmol) was added. The mixture was stirred at room temperature for 18 h until the consumption of starting material, and then, it was acidified with acetic acid to pH 3 and diluted with CH_2Cl_2. The solution was washed with water, dried ($MgSO_4$), and concentrated in vacuo. Concentration gave compound **29** as a white solid (15 mg, 66%); mp 183−184 °C. IR (neat) ν_{max}/cm^{-1} 3357 (N−H), 2915 (COO−H), 1749 (HOC═O), 1624 (NC═O). ^{1}H NMR (500 MHz; MeOD-d_4): δ 4.25 (2H, s, CH_2), 7.68−7.71 (1H, m, Ar C*H*), 7.82−7.85 (1H, m, Ar C*H*), 8.00 (1H, d, J = 8.0, Ar C*H*), 8.19 (2H, t, J = 8.5, Ar C*H*), 8.47 (1H, d, J = 8.5, Ar C*H*). ^{13}C NMR (125 MHz, DMSO-d_6): δ 42.1 (CH_2), 119.5 (Ar *C*H), 129.0 (Ar *C*H), 129.4 (Ar *C*H), 130.8 (Ar *C*H), 130.85, 131.5 (Ar *C*H), 138.9 (Ar *C*H), 148.1, 150.5, 167.2 (CONH), 172.9 (CO_2H). HRMS (ESI$^-$) $C_{12}H_{10}N_2O_3$ [M − H]$^-$ requires 229.0619; found, 229.0611.

AlkB Expression and Purification. AlkB and ΔN11 AlkB proteins were expressed and purified as described.[23,25] BL21 (DE3) *E. coli* transformed with pET24a AlkB or ΔN11 AlkB were grown at 37 °C and 220 rpm to an OD_{600} of 0.6. Protein expression was induced by the addition of 0.2 mM IPTG (Melford Laboratories Ltd.). Growth was continued at 28 °C for 4 h (AlkB) or 15 °C for 16 h (ΔN11 AlkB), and then, cells were harvested by centrifugation. The resulting cell pellet was stored at −80 °C. Cell pellets were resuspended to homogeneity in 0.1 M MES, pH 5.8, 1 mM $MgCl_2$, and 1× Roche complete EDTA-free protease inhibitor cocktail. Cells were lysed on ice by sonication, and the lysate was cleared by centrifugation and filtration. AlkB was purified from the crude cell lysate by cation exchange chromatography using a 50 mL S sepharose column, with elution achieved by application of a gradient to 1 M NaCl. Further purification was achieved by gel filtration using a 300 mL Superdex 75 column (Pharmacia) in a buffer of 50 mM HEPES, pH 7.5.

Nondenaturing ESI-MS. All 37 thiols used for DCL generation were from Sigma-Aldrich or Alfa Aesar. AlkB was desalted using a Bio-Spin 6 Column (Bio-Rad, Hemel Hempstead, United Kingdom) in 15 mM ammonium acetate (pH 7.5). The stock solution was diluted with the same buffer to a final concentration of 100 μM. $FeSO_4{\cdot}7H_2O$ was dissolved in 20 mM HCl at a concentration of 100 mM. This was then diluted with Milli-Q water to give final working concentrations of 500 μM. The protein was mixed with Fe(II) and an inhibitor to give final concentrations of 15 μM AlkB, 75 μM Fe(II), and 15 μM inhibitor. The solution was then incubated for 30 min at room temperature prior to ESI-MS analysis.

Mass spectrometric data were acquired using a Q-TOF mass spectrometer (Q-TOF micro, Micromass, Altrincham, United Kingdom) interfaced with a NanoMate (Advion Biosciences, Ithaca, NY) with a chip voltage of 1.70 kV and a delivery pressure 0.25 psi. The sample cone voltage was typically 80 V with a source temperature of 40 °C and with an acquisition/scan time of 10 s/1 s. Calibration and sample acquisition were performed in the positive ion mode in the range of 500−5000 m/z. The pressure at the interface between the atmospheric source and the high vacuum region was fixed at 6.60 mbar. External instrument calibration was achieved using sodium iodide. Data were processed with the MassLynx 4.0 (Waters).

DSF. DSF was performed using a MiniOpticon Real-Time PCR Detection System (Bio-Rad), monitoring protein unfolding using SYPRO orange (Invitrogen) according to reported method.[26] FAM (492 nm) and ROX (610 nm) filters were used for excitation and emission, respectively. Reaction mixes contained 2 μM protein, 50 μM Mn(II), 200 μM compounds, and 1× SYPRO orange in a final volume of 50 μL. Reagents were prepared in HEPES buffer except metals, which were dissolved as 100 mM stocks in 20 mM HCl, and then further diluted in Milli-Q water. Compounds tested were prepared in 100% DMSO and added such that the final concentration of DMSO was 5% (v/v).

Fluorescence readings were taken every 1 °C in the range 25−95 °C, with the temperature increased linearly by 1 °C min^{-1}. The software provided was used to perform global minimum subtraction. The inflection point, representing T_m, was calculated by fitting the Boltzmann equation to the sigmoidal curves obtained; data were processed using GraphPad Prism 5.0. The T_m shift caused by the addition of small molecules/fragments was determined by subtraction of the "reference" T_m (protein incubated with metal and 5% DMSO) from the T_m obtained in the presence of the compound.[35] Conditions were tested in triplicate, with standard deviations typically <1 °C.

Inhibition Assays for AlkB.[27,28] Synthetic fluorescently labeled DNA substrate (5′-TTC$_m$TTTTTTTTTTT-3′-fluorescein) and product (5′-TTCTTTTTTTTTTTT-3′-fluorescein) were produced by ATDBio (University of Southampton, United Kigndom). All other chemicals were purchased from Sigma-Aldrich (Toronto, ON). An uncoated fused-silica capillary was purchased from Polymicro Technologies (Phoenix, AZ). All solutions were made using deionized water filtered through a 0.22 μm filter (Millipore, Nepean, ON).

All experiments were conducted using an uncoated fused silica capillary with a total length of 50 cm (40 cm to the detection window), inner diameter of 75 μm, and outer diameter of 365 μm. The capillary

was mounted on a P/ACE MDQ capillary electrophoresis (CE) instrument (Beckman Coulter, Fullerton, CA) with temperature control to keep the capillary at 15 °C. A sample was introduced into the capillary by a pressure pulse of 0.5 psi for 5 s. The reaction product (P) and substrate (S) were then separated by CE at 20 kV and quantitated with laser-induced fluorescence (LIF) detection (fluorescence excitation at 488 nm and fluorescence detection at 520 nm). The CE run buffer for kinetic and inhibition studies was 20 mM Borax and 60 mM SDS at pH 8.0.

The enzymatic reaction was initiated by the addition of AlkB protein to a mixture containing the incubation buffer (50 mM Tris-HCl, pH 7.5), 4 mM AA, 160 μM 2OG, 80 μM $(NH_4)_2SO_4·FeSO_4·6H_2O$, 100 nM 5′-TTC$_m$TTTTTTTTTTT-3′-fluorescein, and 2154 units of catalase. The relative activity of AlkB was measured using 5 nM AlkB and 100 nM oligonucleotide substrate, while varying the inhibitor concentration in the range 1−1000 μM. The enzymatic reactions were incubated for 4.5 min at room temperature and stopped by adding a prechilled EDTA solution (5 mM final concentration). The demethylated DNA product formed was separated from the unreacted substrate by CE and quantified with LIF. The relative activity of AlkB at different inhibitor concentrations was plotted against the inhibitor concentration, and the IC_{50} values were calculated as the concentration of inhibitor reducing the enzymatic activity to half its maximal level, using the OriginPro 8.0 software.

Inhibition Assays for PHF8[33] and PHD2. Reactions consisted of PHF8 (2 μM), Fe(II) (10 μM), ascorbate (100 μM), 2OG (20 μM) H3(1−14)K4me3K9me2 peptide (20 μM), and inhibitor (1 mM) in 1% DMSO, 500 mM NaCl, 100 mM HEPES (pH 7.5). PHF8, Fe(II), ascorbate, and inhibitors were preincubated at 37 °C for 15 min before the addition of 2OG and peptide. Reactions were incubated at 37 °C for 20 min prior to 1:1 quenching with methanol. Product formation was assessed by MALDI-TOF; 1 μL of quenched reaction was mixed with 1 μL of α-cyano-4-hydroxycinnamic acid and spotted onto a MALDI-TOF plate for analysis.[33] Inhibition levels were measured relative to an inhibitor free reaction. Inhibition assay methods for PHD2 will be reported elsewhere. Details of the N terminally truncated PHD2 was prepared as reported.[36,37]

Protein Crystallography. Crystals of AlkB in complex with **15**, **18**, and **22** were grown in sitting drops at 293 K using vapor diffusion methods. The ratio of protein to reservoir solution for the AlkB:**15** and AlkB:**18** cocrystallization drops was 2:1 (300 nL total drop volume) and for AlkB:**22** was 1:1 (200 nL total drop volume), and the reservoir volume was 80 μL. The AlkB protein solution contained 10.1 mg/mL protein, 50 mM HEPES, pH 7.5, 2.2 mM ammonium iron(II) sulfate, and 5.7 mM **15** or 1 mM **18**. The protein solution for the AlkB:**22** complex contained the same except that the ammonium iron(II) sulfate concentration was 0.44 mM and **22** was 1 mM. The reservoir solution for AlkB:**15** contained 0.2 M sodium chloride, 0.1 M HEPES, pH 7.5, and 25% w/v polyethylene glycol (PEG) 3350; for AlkB:**18**, 0.2 M ammonium sulfate, 0.1 M tris-hydrochloride, pH 8.5, and 25% w/v PEG 3350; for AlkB:**22**, 0.1 M bis-tris, pH 6.5, and 25% w/v PEG 3350. The crystals were cryocooled using well solution diluted to 25% v/v glycerol and flash cooled in an Oxford Cryosystems nitrogen gas stream. Data were collected from a single crystal at 100 K using a Rigaku FR E+ Superbright diffractometer equipped with a copper rotating anode, Osmic HF optics, and a Saturn 944+ CCD detector. The data were indexed, integrated, and scaled using HKL2000,[38] and the structure was determined by molecular replacement using the AutoMR (PHASER)[39] subroutine in PHENIX[40] with 2FDJ (PDB ID)[25] as a search model for AlkB:**15** and 3T4H (PDB ID) as a search model for AlkB:**18** and AlkB:**22**. Iterative rounds of model building and refinement using COOT[41] and PHENIX[41] were performed until the decreasing R and R_{free} no longer converged. The final R factors for the models were as follows: AlkB:**15**, R = 15.9% and R_{free} = 18.7%; AlkB:**18**, R = 16.1% and R_{free} = 20.2%; and AlkB:**22**, R = 18.2% and R_{free} = 22.1%.

■ ASSOCIATED CONTENT

Ⓢ Supporting Information

Chemical synthesis and compound characterizations, statistical analyses on correlations between ESI-MS, thermal shift and inhibition data, nondenaturing ESI-MS binding experiments, and crystallographic structure solution methods. This material is available free of charge via the Internet at http://pubs.acs.org.

Accession Codes

The coordinates for AlkB in complex with **15**, **18**, and **22** have been deposited in the RCSB Protein Data Bank as PDB IDs 3T4H, 3T4V, and 3T3Y, respectively.

■ AUTHOR INFORMATION

Corresponding Author

*Tel: +44(0)1865 275 625. Fax: +44(0)1865 285 022. E-mail: Christopher.schofield@chem.ox.ac.uk.

Present Address

∥Department of Pharmacy, National University of Singapore, 18 Science Drive 4, Singapore 117543, Singapore.

Author Contributions

⊥These authors contribute equally to this work.

Notes

The authors declare no competing financial interest.

■ ACKNOWLEDGMENTS

We thank Pfizer Limited, the Biotechnology and Biological Sciences Research Council, and the Wellcome Trust for funding our work.

■ ABBREVIATIONS USED

2OG, 2-oxoglutarate; FTO, fat mass and obesity protein; TET, Ten-Eleven-Translocation protein; PHF8, PHD finger protein 8; PHD2, hypoxia-inducible factor prolyl hydroxylase 2; DCMS, dynamic combinatorial mass spectrometry; ESI-MS, electrospray ionization mass spectrometry; DSF, differential scanning fluorimetry; T_m, melting temperature; rmsd, root-mean-square deviation

■ REFERENCES

(1) Wu, S. C.; Zhang, Y. Active DNA demethylation: many roads lead to Rome. *Nat. Rev. Mol. Cell Biol.* **2010**, *11*, 607−620.

(2) Sedgwick, B.; Bates, P. A.; Paik, J.; Jacobs, S. C.; Lindahl, T. Repair of alkylated DNA: Recent advances. *DNA Repair* **2007**, *6*, 429−442.

(3) Sancar, A. DNA repair in humans. *Annu. Rev. Genet.* **1995**, *29*, 69−105.

(4) Vaughan, P.; Sedgwick, B.; Hall, J.; Gannon, J; Lindahl, T. Environmental mutagens that induce the adaptive response to alkylating agents in *Escherichia coli*. *Carcinogenesis* **1991**, *12*, 263−268.

(5) Trewick, S. C.; Henshaw, T. F.; Hausinger, R. P.; Lindahl, T.; Sedgwick, B. Oxidative demethylation by E. coli alkB directly reverts DNA base damage. *Nature* **2002**, *419*, 174−178.

(6) Schofield, C. J.; Zhang, Z. Structural and mechanistic studies on 2-oxoglutarate-dependent oxygenases and related enzymes. *Curr. Opin. Struct. Biol.* **1999**, *9*, 722−731.

(7) Delaney, J. C.; Essigmann., J. M. Mutagenesis, genotoxicity, and repair of 1-methyladenine, 3-alkylcytosines, 1-methylguanine, and 3-methylthymine in alkB Escherichia coli. *Proc. Natl. Acad. Sci. U.S.A.* **2004**, *101*, 14051−14056.

(8) Delaney, J. C.; Smeester, L.; Wong, C.; Frick, L. E.; Taghizadeh, K.; Wishnok, J. S.; Drennan, C. L.; Samson, L. D.; Essigmann, J. M. AlkB reverses etheno DNA lesions caused by lipid oxidation in vitro and in vivo. *Nat. Struct. Mol. Biol.* **2005**, *12*, 855−860.

(9) Tsujikawa, K.; Koike, K.; Kitae, K.; Shinkawa, A.; Arima, H.; Suzuki, T.; Tsuchiya, M.; Makino, M.; Furukawa, T.; Konishi, N.; Yamamoto, H. Expression and sub-cellular localization of human ABH family molecules. *J. Cell. Mol. Med.* **2007**, *11*, 1105−1116.
(10) Ringvoll, J.; Nordstrand, L. M.; Vagbo, C. B.; Talstad, V.; Reite, K.; Aas, P. A.; Lauritzen, K. H.; Liabakk, N. B.; Bjork, A.; Doughty, R. W.; et al. Repair deficient mice reveal mABH2 as the primary oxidative demethylase for repairing 1meA and 3meC lesions in DNA. *EMBO J.* **2006**, *25*, 2189−2198.
(11) Born, E. V. D.; Vågbø, C. B.; Songe-Møller, L.; Leihne1, V.; Lien, G. F.; Leszczynska, G.; Malkiewicz, A.; Krokan, H. E.; Kirpekar, F.; Klungland, A.; Falnes, P. Ø. ALKBH8-mediated formation of a novel diastereomeric pair of wobble nucleosides in mammalian tRNA. *Nat. Commun.* **2011**, *2*, article number 172.
(12) Frayling, T. M.; et al. A Common Variant in the *FTO* Gene Is Associated with Body Mass Index and Predisposes to Childhood and Adult Obesity. *Science* **2007**, *316*, 889−894.
(13) Gerken, T.; Girard, C. A.; Tung, Y. C.; Webby, C. J.; Saudek, V.; Hewitson, K. S.; et al. The obesity-associated FTO gene encodes a 2-oxoglutarate-dependent nucleic acid demethylase. *Science* **2007**, *318*, 1469−1472.
(14) Jia, G.; Yang, C.-G.; Yang, S.; Jian, X.; Yi, C.; Zhou, Z.; He, C. Oxidative demethylation of 3-methylthymine and 3-methyluracil in single-stranded DNA and RNA by mouse and human FTO. *FEBS Lett.* **2008**, *582*, 3313−3319.
(15) Tahiliani, M.; Koh, K. P.; Shen, Y.; Pastor, W. A.; Bandukwala, H.; Brudno, Y.; Agarwal, S.; Iyer, L. M.; Liu, D. R.; Aravind, L.; Rao, A. Conversion of 5-Methylcytosine to 5-Hydroxymethylcytosine in Mammalian DNA by MLL Partner TET1. *Science* **2009**, *324*, 930−935.
(16) Ito, S.; Shen, L.; Dai, Q.; Wu, S. C.; Collins, L. B.; Swenberg, J. A.; He, C.; Zhang, Y. Tet Proteins Can Convert 5-Methylcytosine to 5-Formylcytosine and 5-Carboxylcytosine. *Science* DOI: 10.1126/science.1210597.
(17) Thalhammer, A.; Hansen, A. S.; El-Sagheer, A. H.; Brown, T.; Schofield, C. J. Hydroxylation of methylated CpG dinucleotides reverses stabilisation of DNA duplexes by cytosine 5-methylation. *Chem. Commun.* **2011**, *47*, 5325−5327.
(18) Rose, N. R.; Woon, E. C. Y.; Kingham, G. L.; King, O. N. F; Mecinović, J.; Clifton, I. J.; Ng, S. S.; Talib-Hardy, J.; Oppermann, U.; McDonough, M. A.; Schofield, C. J. Selective Inhibitors of the JMJD2 Histone Demethylases: Combined Nondenaturing Mass Spectrometric Screening and Crystallographic Approaches. *J. Med. Chem.* **2010**, *53*, 1810−1818.
(19) Liénard, B. M. R.; Hüting, R.; Lassaux, P.; Galleni, M.; Frère, J.-M.; Schofield, C. J. Dynamic combinatorial mass spectrometry leads to metallo-beta-lactamase inhibitors. *J. Med. Chem.* **2008**, *51*, 684−688.
(20) Liénard, B. M. R.; Selevsek, N.; Oldham, N. J.; Schofield, C. J. Combined mass spectrometry and dynamic chemistry approach to identify metalloenzyme inhibitors. *ChemMedChem* **2007**, *2*, 175−179.
(21) Poulsen, S.-A. Direct screening of a dynamic combinatorial library using mass spectrometry. *J. Am. Soc. Mass Spectrom.* **2006**, *17*, 1074−1080.
(22) Daniel, J. M.; Friess, S. D; Rajagopalan, S.; Wendt, S.; Zenobi, R. Quantitative determination of noncovalent binding interactions using soft ionization mass spectrometry. *Int. J. Mass Spectrom.* **2002**, *216*, 1−27.
(23) Welford, R. W. D.; Schlemminger, I.; McNeill, L. A.; Hewitson, K. S.; Schofield, C. J. The Selectivity and Inhibition of AlkB. *J. Biol. Chem.* **2003**, *278*, 10157−10161.
(24) McDonough, M. A.; McNeill, L. A.; Tilliet, M.; Papamicael, C. A.; Chen, Q. Y.; Banerji, B.; Hewitson, K. S.; Schofield, C. J. Selective inhibition of factor inhibiting hypoxia-inducible factor. *J. Am. Chem. Soc.* **2005**, *127*, 7680−7681.
(25) Yu, B.; Edstrom, W. C.; Benach, J.; Hamuro, Y.; Weber, P. C.; Gibney, B. R.; Hunt, J. F. Crystal structures of catalytic complexes of the oxidative DNA/RNA repair enzyme AlkB. *Nature* **2006**, *439*, 879−884.
(26) Niesen, F. H.; Berglund, H.; Vedadi, M. The use of differential scanning fluorimetry to detect ligand interactions that promote protein stability. *Nat. Protoc.* **2007**, *2*, 2212−2221.
(27) Karkhanina, A. A.; Mecinovic, J.; Musheev, M. U.; Krylova, S. M.; Petrov, A. P.; Hewitson, K. S.; Flashman, E.; Schofield, C. J.; Krylov, S. N. Direct Analysis of Enzyme-Catalyzed DNA Demethylation. *Anal. Chem.* **2009**, *81*, 5871−5875.
(28) Krylova, S. M.; Karkhanina, A. A.; Musheev, M. U.; Bagg, E. A.; Schofield, C. J.; Krylov, S. N. DNA aptamers for as analytical tools for the quantitative analysis of DNA-dealkylating enzymes. *Anal. Biochem.* **2011**, *414*, 261−265.
(29) Rose, N. R; McDonough, M. A.; King, O. N. F.; Kawamura, A.; Schofield, C. J. Inhibition of 2-oxoglutarate dependent oxygenases. *Chem. Soc. Rev.* **2011**, *40*, 4364−4397.
(30) Yu, B.; Hunt, J. F. Enzymological and structural studies of the mechanism of promiscuous substrate recognition by the oxidative DNA repair enzyme AlkB. *Proc. Natl. Acad. Sci. U.S.A.* **2009**, *106*, 14315−14320.
(31) Loenarz, C.; Schofield, C. J. Expanding chemical biology of 2-oxoglutarate oxygenases. *Nat. Chem. Biol.* **2008**, *4*, 152−156.
(32) Schofield, C. J.; Ratcliffe, P. J. Oxygen sensing by HIF hydroxylases. *Nat. Rev. Mol. Cell Biol.* **2004**, *5*, 343−354.
(33) Loenarz, C.; Ge, W.; Coleman, M. L.; Rose, N. R.; Cooper, C. D. O.; Klose, R. J.; Ratcliffe, P. J.; Schofield, C. J. *PHF8*, a gene associated with cleft lip/palate and mental retardation, encodes for an N^{ε}-dimethyl lysine demethylase. *Hum. Mol. Genet.* **2010**, *19*, 217−222.
(34) Weidmann, K.; Baringhaus, K.-H.; Tschank, G. Bickel, 3-hydroxypyridine-2-carboxamidoesters, their preparation and their use as pharmaceuticals. M. Eur. Pat. Appl. EP 765871 A1 19970402, 1997.
(35) Davis, J. W. Jr. Studies with quinolines. I. Synthesis of quinaldic acid and some of its amide derivatives. *J. Org. Chem.* **1959**, *24*, 1691−1694.
(36) McDonough, M. A.; Li, V.; Flashman, E.; Chowdhury, R.; Mohr, C.; Lienard, B. M. R.; Zondlo, J.; Oldham, N. J.; Clifton, I. J.; Lewis, J.; McNeill, L. A.; Kurzeja, R. J. M.; Hewitson, K. S.; Yang, E.; Jordan, S.; Syed, R. S.; Schofield, C. J. Cellular oxygen sensing: Crystal structure of hypoxia-inducible factor prolyl hydroxylase (PHD2). *Proc. Natl. Acad. Sci. U.S.A.* **2006**, *103*, 9814−9819.
(37) McNeill, L. A.; Flashman, E.; Buck, M. R. G.; Hewitson, K. S.; Clifton, I. J.; Jeschke, G.; Claridge, T. D. W.; Ehrismann, D.; Oldham, N. J.; Schofield, C. J. Hypoxia-inducible factor prolyl hydroxylase 2 has a high affinity for ferrous iron and 2-oxoglutarate. *Mol BioSyst.* **2005**, *1*, 321−324.
(38) Otwinowski, Z.; Minor, W. In *Methods in Enzymology*; Elsevier: 1997; Vol. *276*, pp 307−326.
(39) McCoy, A. J.; Grosse-Kunstleve, R. W.; Adams, P. D.; Winn, M. D.; Storoni, L. C.; Read, R. J. Phaser crystallographic software. *J. Appl. Crystallogr.* **2007**, *40*, 658−674.
(40) Adams, P. D.; Afonine, P. V.; Bunkóczi, G.; Chen, V. B.; Davis, I. W.; Echols, N.; Headd, J. J.; Hung, L.-W.; Kapral, G. J.; Grosse-Kunstleve, R. W.; McCoy, A. J.; Moriarty, N. W.; Oeffner, R.; Read, R. J.; Richardson, D. C.; Richardson, J. S.; Terwilliger, T. C.; Zwart, P. H. PHENIX: A comprehensive Python-based system for macromolecular structure solution. *Acta Crystallogr., Sect. D: Biol. Crystallogr.* **2010**, *66*, 213−221.
(41) Emsley, P.; Cowtan, K. Coot: Model-building tools for molecular graphics. *Acta Crystallogr., Sect. D: Biol. Crystallogr.* **2004**, *60*, 2126−2132.